Fine cohesive powders in rotating drums: Transition from rigid-plastic flow to gas-fluidized regime

A. Castellanos, J. M. Valverde, and M. A. S. Quintanilla
Departamento de Electronica y Electromagnetismo, Universidad de Sevilla, Avenida Reina Mercedes s/n, 41012 Sevilla, Spain
(Received 28 November 2001; published 12 June 2002)

We investigate the dynamics of fine cohesive powders inside rotating drums. We show that these powders may be fluidized due to entrapment of ambient gas, and we determine the onset of fluidization. Experimental measurements on the bed expansion as a function of the rotation velocity have been performed. Drums of different diameters and fine powders of varying cohesiveness have been tested. We show that (i) fine powders transit directly from a rigid-plastic state to a gas-fluidized state in accordance with the flow regime boundaries predicted elsewhere [A. Castellanos *et al.*, Phys. Rev. Lett. **82**, 1156 (1999)], (ii) the onset of fluidization in the rotating drum is determined by the ratio of the powder kinetic energy per unit volume to its tensile strength, and (iii) once the powder is completely fluidized the average interstitial gas velocity increases proportionally to the rotation velocity. The last two results imply that the required velocity to fluidize a powder, ωR (ω angular velocity, R radius of the drum), must increase as the square root of its tensile strength, and this has been confirmed by independent measurements and estimations.

DOI: 10.1103/PhysRevE.65.061301 PACS number(s): 45.70.−n, 47.55.Kf, 47.55.Mh

I. INTRODUCTION

Problems with powder flowability are very important in industrial applications involving powder transportation and mixing. Powders in plastic flow exhibit low flowability and poor mixing, and it is common practice in industry to flow gas through these powders in order to enhance the above mentioned properties. Fortunately, in many industrial devices that use mechanical moving parts the ambient gas may be entrapped in the powder thus facilitating its transport and mixing. Due to this, the behavior of fine powders in rotating drums displays quite different features from noncohesive grains, as already observed a long time ago by Rietema [1].

The particle size, ranging from less than 1 μm to 1000 μm or more, constitutes a critical parameter in the flow behavior of granular materials [2]. At low stresses granular assemblies exhibit the solid-plastic regime, resisting shear by undergoing plastic deformations. When the limit of plastic stability is reached, noncohesive granular materials such as dry sand (particle diameter $\gtrsim 100$ μm), display an inertial regime, where stresses are mainly carried by interparticle collisions. This high shear rate flow has been often investigated in a horizontal rotating drum partially filled with the granular sample [3]. In such device intermittent quasiperiodic avalanches of grains are observed for low rotation speeds [4]. As the rotation velocity ω is increased the frequency of the avalanches increases until a continuously cascading superficial layer of ~ 10 grains is formed, feeded by the rest of the grains that undergo rigid-body rotation [5]. The slope of the surface increases with ω due to inertial forces and at higher velocities, the steady profile of the free surface takes the form of a tilted ''S.''

On the contrary, fine powders (particle diameter d_p between ~ 1 μm and ~ 100 μm) do not exhibit the inertial regime but experience a direct transition from the solid-plastic to the fluidized regime due to the strong interaction between particles and interstitial air [2]. At very low rotation rates quasiperiodic avalanches may be observed, but as opposed to noncohesive grains, these avalanches are of a typical depth correlated to powder cohesiveness and boundary conditions and much larger than particle size [6]. In this rigid-plastic regime these fine dry powders are akin to wet sand more than to dry sand. However, they differ from wet sand in one important respect. As we increase the angular velocity the rate of avalanching increases. During the avalanching process the surrounding gas is entrained in the bulk. In addition the falling material wedge may be partially fluidized upon impact on the drum wall. As a result the surrounding gas is more and more entrained in the bulk as we increase the angular velocity and radius of the drum. The entrained gas takes a time to leave the fluidized powder that may be eventually larger than the time interval between successive avalanches for high enough rotation velocities. Then a permanent fluidized region appears at the lower part of the slope, whereas the rest of the powder remains in the solid-plastic regime. The fluidized region grows with the rotation velocity until the whole material becomes fluidized. At this stage the free surface becomes horizontal resembling the behavior of a low viscosity liquid (see Fig. 1). If the rotation velocity is further increased beyond the onset of full fluidization the powder is further expanded. The objective of this paper is to determine the parameters on which this transition depends in order to gain an understanding of the underlying physical process. In a first part of the present work the effects of powder cohesion and drum diameter on the onset of fluidization of fine particles in rotating drums are investigated.

Another device used to investigate the properties of powders has been described previously [7], a schematic of which is shown in Fig. 2. It consists of a vertical vessel closed at the bottom by a porous plate. A controlled gas flow is supplied from below to a bed of powder particles partially filling the vessel and the gas pressure drop across the powder is measured by a differential pressure transducer. The bed height is read from an ultrasonic sensor and from this data the solid volume fraction is calculated. With sufficiently high gas flow the upward drag force exerted by the gas on the particles counteracts gravity and interparticle cohesive forces, allowing us to measure the tensile strength of the

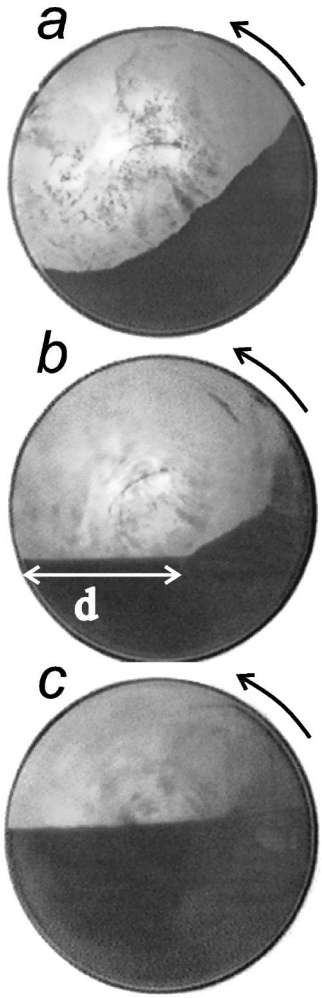

FIG. 1. Experimental profiles of the flow of a xerographic toner in a rotating drum at increasing values of the rotation velocity (10 rpm, 45 rpm, and 100 rpm).

sample (see [7] for details on the measurement process). Further increase in the flow causes the bed to expand homogeneously and stable fluidization occurs. Using such a device it is possible to analyze the relationship between the fluidizing gas velocity and the solid volume fraction of the fluidized bed as a function of powder cohesiveness [8]. A second part of the present work will consist of relating the average interstitial gas velocity in the rotating drum to the rotation speed. To this end, data from the powder bed technique will be employed.

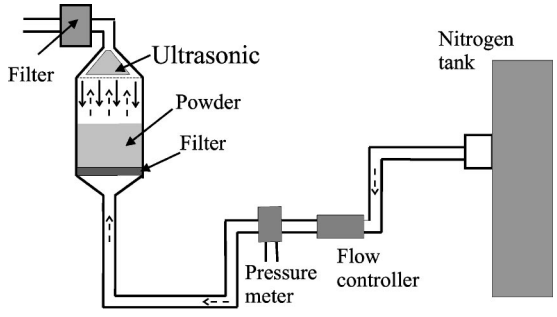

FIG. 2. Experimental setup of the powder bed technique.

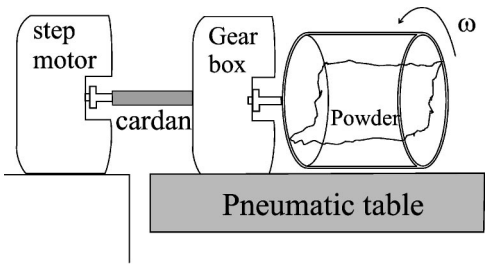

FIG. 3. Experimental setup of the rotating drum experiment.

II. EXPERIMENTAL SETUP

In the experiments we used a computer controlled step motor to rotate polycarbonate drums of several diameters ($D=42$ mm, 50 mm, and 90 mm internal diameters, and 40 mm length). The drum was placed on an air table and connected to the motor by an elastic cardan to isolate it from any external vibration (see Fig. 3). To record the experiment a charge-coupled device (CCD) camera was interfaced to a computer and controlled with an image processing software. In all our measurements we begin by initializing the sample, which we do by fluidizing the powder. To fluidize the powder the drum is driven to an angular velocity around 200 rpm. Once the powder reaches a stationary fluidized state the drum is suddenly stopped and the powder is allowed to collapse under gravity. In this way a very reproducible consolidation state of the powder is obtained. Then the rotation speed is slowly increased from zero to 200 rpm and the volume fraction of the drum occupied by the powder (f) and length of the free surface of the fluidized region (d, see Fig. 1) are computed using an image software.

III. MATERIALS

Measurements have been performed on a range of xerographic toners made from polymer (particle density $\rho_p \simeq 1$ g/cm^3). Powders of varying particle size have been tested (4.4, 7.2, and 12.7 μm) blended with different amounts of surface additives such as Aerosil^R and Cab-o-sil^R (nanoparticles of fumed silica), well known for their ability to diminish interparticle adhesion forces. Experiments have been also carried out using a low cohesiveness commercially available toner (Canon CLC 700). van der Waals attractive forces are dominant between our uncharged and dry fine particles. The addition of nanoparticles results in a reduction in the powder tensile strength because the additives are made of a hard material and therefore they increase the hardness of the contacts; they also reduce the powder tensile strength by reducing the size of the contacts. Another important parameter affecting the tensile strength through its effect on the packing fraction and the contact area between particles is the consolidation stress (weight per unit area). As a general rule the tensile strength increases with the consolidation stress. Furthermore the rate of increase is a decreasing function of the amount of additives (see [9] and references therein). The tensile strength may increase dramatically with the consolidation time, indicating viscoplastic deformation of the particle contact area [10]. To rule out the influence of this effect,

TABLE I. Physical properties of xerographic toners used in the experiments with drums of different diameters. The concentration of additive is given in wt. %, d_p is the average particle size, D is the drum internal diameter. ϕ_0 is the solid volume fraction of the powder, partially and uniformly filling the static drum, and σ_t is the corresponding tensile strength, measured by means of the powder bed technique [7].

Sample no.	$d_p(\mu\text{m})$	Additive (%)	D (cm)	ϕ_0	σ_t (Pa)
a	12.7	0.4	9	0.4	25
b	12.7	0.4	5	0.4	28
c	12.7	0.4	4.2	0.38	16
d	12.7	0.02	9	0.31	58
e	12.7	0.02	5	0.32	70
f	12.7	0.2	4.2	0.33	26
g	12.7	0.1	4.2	0.33	48
h	8.5		9	0.34	20
i	8.5		5	0.34	20
j	7.2	2	9	0.41	36
k	7.2	2	5	0.4	30
l	4.4	2	9	0.39	25
m	4.4	2	5	0.37	16

all tests have been performed within the first 5 m after settling. A summary of the relevant physical properties for our purposes of the samples tested in this work is given in Table I.

IV. RESULTS

Figures 4 and 5 display f/f_0 (where f_0 is the initial volume fraction) and d/D as a function of ω. As anticipated, both f/f_0 and d/D increase with the rotation speed, but are also strong functions of the powder cohesiveness and drum diameter. Indeed, the trend followed by f/f_0 and d/D with σ_t and D might be expected. On one hand, decreasing the tensile strength decreases the minimum interstitial gas velocity for fluidization and this facilitates fluidization and the consequent further expansion of the bed. This is evident from the different behavior of samples *a*-*d*, *b*-*e*, and *c*-*f*-*g*, in Figs. 4 and 5; these samples differ only in their tensile strength, and we may see that the smaller the tensile strength the faster is the transition to the fluidized state. On the other hand, the interstitial gas velocity would also be increased by the increase in the tangential velocity when using larger drums, thus facilitating fluidization. Again this can be verified by looking at samples *a*-*b*, *d*-*e*, *h*-*i*, *j*-*k*, and *l*-*m*. Each pair consist of the same powder, and differ only in the diameter of the rotating drum, which is 9 cm for the first member of the pair and 5 cm for the second member. As it is apparent the first member of the pair shows a faster increase in both f/f_0 and d/D.

V. DISCUSSION

Let us now search for the main parameters governing fluidization in the rotating drum. From the three variables involved in the problem, namely, the powder tensile strength

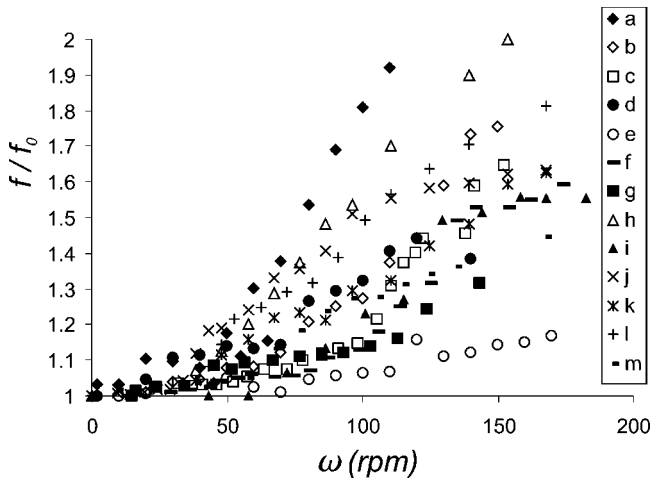

FIG. 4. Ratio of the volume fraction of the drum occupied by the powder to the initial volume fraction as a function of the angular rotation velocity.

σ_t, drum radius $R=D/2$, and rotation velocity ω, two nondimensional parameters may be derived. A simple choice are the Froude number (ratio of centrifugal acceleration to gravity acceleration), $\text{Fr}=\omega^2 R/g$, and the ratio of σ_t to the typical potential energy density $\rho g R$, where ρ is the powder density, $\text{Co}=\sigma_t/\rho g R$, named hereafter cohesion number. Thus, both f/f_0 and d/D must be certain functions of Fr and Co,

$$f/f_0 = G(\text{Fr}^{\alpha},\text{Co}^{\beta}), \tag{1}$$

$$d/D = H(\text{Fr}^{\delta},\text{Co}^{\gamma}). \tag{2}$$

In the limit $\omega \to 0$, it must be $f \to f_0$ and $d \to 0$, and this leads us to hypothesize the simple dependence

$$f/f_0 = 1 + A\text{Fr}^{\alpha}\text{Co}^{\beta}, \tag{3}$$

$$d/D = B\text{Fr}^{\delta}\text{Co}^{\gamma}, \tag{4}$$

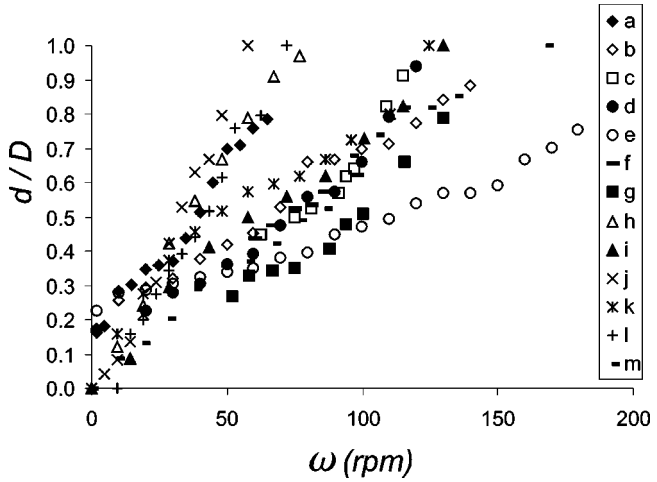

FIG. 5. Length of the horizontal part of the free surface of the powder as a function of the rotation velocity.

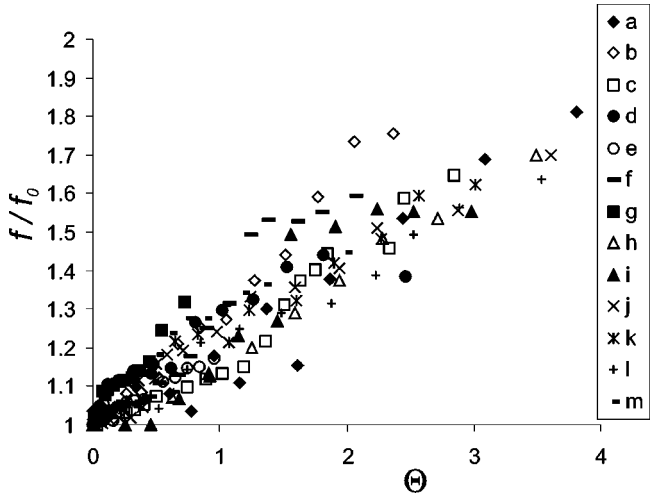

FIG. 6. Ratio of the volume fraction of the drum occupied by the powder to the initial volume fraction as a function of the ratio of kinetic energy density to powder tensile strength.

where $\alpha>0$ and $\delta>0$, and A and B are proportionality constants. Experimental data of f/f_0 for the whole set of powders investigated fit pretty well to the proposed law for $\alpha=0.97\pm0.27$ and $\beta=-1.07\pm0.28$, which are the best fit parameters from a regression analysis (see Fig. 6). Approximating $\alpha\simeq1$ and $\beta\simeq-1$ we have $f/f_0\simeq1+A\mathrm{Fr}/\mathrm{Co}=1+A\Theta$, where a new nondimensional parameter $\Theta=\rho\omega^2R^2/\sigma_t$ has arisen. Since d/D is a measure of the longitudinal extent of the fluidized region and f/f_0 is a measure of the area (the drum height is held constant), we might anticipate $d/D\propto\sqrt{\Theta}$. Figure 7 shows d/D as a function of $\sqrt{\Theta}$. It can be seen that d/D increases linearly with $\sqrt{\Theta}$ as expected. Moreover, the condition for full fluidization can be established as $d\approx D$, and, from Fig. 7, this happens for $\Theta^{1/2}\sim1$. Alternatively, the expansion of the powder can be measured by the decrease of its solid volume fraction ϕ related to the volume fraction by $f/f_0=\phi_0/\phi$, ϕ_0 being the initial solid volume fraction of the powder. Therefore, the relative decrease of the solid volume fraction $(\phi_0-\phi)/\phi$ is

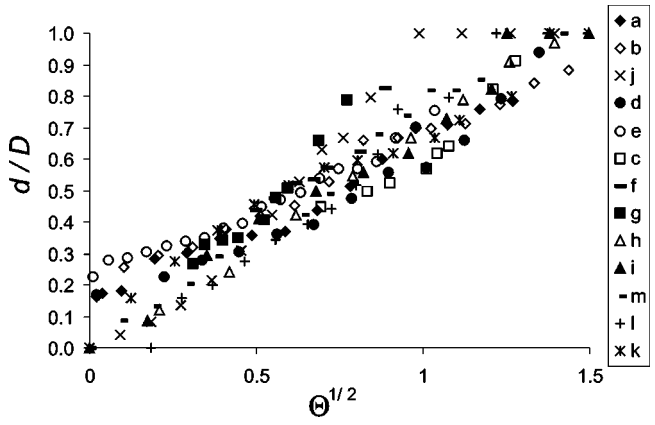

FIG. 7. Length of the horizontal part of the free surface of the powder as a function of the square root of the ratio of the kinetic energy density to the tensile strength.

TABLE II. Number of aggregated particles and fractal dimension of aggregates derived from settling experiments [12] for the different powders used in this study and characterized by their average particle size (d_p) and wt. % of flow additives.

$d_p(\mu\mathrm{m})$	%	N	D_f
12.7	0.2	20	2.64
12.7	0.4	20	2.56
12.7	0.1	22	2.66
12.7	0.02	46	2.5
7.2	2	133	2.7
4.4	2	1300	2.73
8.53(canon)		96	2.62

proportional to Θ. We conclude that fluidization of the powder in the rotating drum is mainly ruled by the nondimensional number Θ.

We now turn to investigate the average interstitial velocity $\langle v_i\rangle$ of the fluidizing gas across the powder. To this end we will make use of the powder bed technique described in [8]. The powder is homogeneously fluidized by flowing a controlled gas flow through the bed and the relation between the solid volume fraction and the interstitial gas velocity is precisely measured. Fine particles in the fluidized state are aggregated due to strong interparticle adhesive forces [11]. Aggregates were modeled as effective particles with a radius of gyration equal to its hydrodynamic radius and characterized by a number of aggregated particles N and a fractal dimension D_f [12]. By means of an extended Richardson-Zaki equation, the settling velocity v_s can be related to the solid volume fraction (ϕ) of the fluidized powder by means of the equation [12]

$$\frac{v_s}{v_a}=(1-\phi_{ef})^n, \tag{5}$$

where v_a is the Stokes settling velocity of a single aggregate ($v_a=v_{p0}N^{1-1/D_f}$, being v_{p0} the settling velocity of a single particle), ϕ_{ef} is the volume fraction occupied by the aggregates ($\phi_{ef}=\phi N^{-1+3/D_f}$), and n a parameter of order 5. Settling experiments served us to establish that the settling velocity of a initially fluidized bed of particles after suddenly stopping the gas flow is equal to the superficial gas velocity v_g in the fluidized state. The interstitial gas velocity in the fluidized bed is then given by $v_i(\phi)=v_s/(1-\phi_{ef})$.

To find N and D_f for each powder investigated in this study experiments on sedimentation have been performed. Results for N and D_f are shown in Table II. As we obtained for other fine powders, D_f approaches closely to the value given by the diffusion limited aggregation model [13] in 3D ($D_f=2.5$) as a consequence of the large interparticle adhesive forces as compared to particle weight [12]. Let us assume that the average interstitial gas velocity in the rotating drum experiment $\langle v_i\rangle$ is of the order of v_i in the fluidized bed when the powder is fluidized in both experiments with the same value of ϕ, i.e., $\langle v_i\rangle(\phi)\simeq v_i(\phi)$. Then Eq. (5) may serve us to estimate $\langle v_i\rangle(\phi)$ and correlate it with the rotation

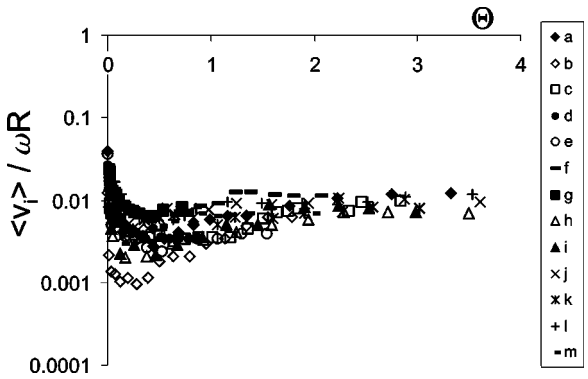

FIG. 8. Ratio of the estimated average interstitial gas velocity in the drum to drum tangential velocity as a function of the ratio of kinetic energy density to powder tensile strength.

speed of the drum. In Fig. 8 we have plotted the ratio of $\langle v_i \rangle$, estimated in this way, to the tangential velocity of the drum ωR. As can be observed, $\langle v_i \rangle / (\omega R) \sim 10^{-2}$ in the region of complete fluidization for all the powders investigated. On the other hand from Fig. 7 we inferred $\Theta \equiv \rho \omega^2 R^2 / \sigma_t \sim 1$ for complete fluidization. Therefore, and because $\rho = \rho_p \phi$ does not change appreciably for our powders, the interstitial gas velocity at fluidization $\langle v_i \rangle$ should scale as the square root of the powder tensile strength σ_t. To check this behavior we have measured the interstitial gas velocity for a homogeneous fluidization state (with $\phi = 0.15$) for several powders of same mass and particle size, only differing in the amount of surface additives. Results are plotted in Fig. 9. It is observed that the interstitial gas velocity can be well fitted by the law $v_i \propto \sqrt{\sigma_t}$, in agreement with our expectation. On the other hand, since the fluidized state is a diluted state, according to Eq. 5 the interstitial gas velocity can be roughly estimated as the aggregate settling velocity $v_i \sim v_a = N^{1-1/D_f}$. According to a power law fit of the data presented in [12], $N^{1-1/D_f} \sim \mathrm{Bo}^{0.43} \simeq \mathrm{Bo}^{0.5}$, where Bo is the ratio of the interparticle adhesion force to the particle weight and labeled Bo because of its similarity to the Bond number in fluid mechanics. For the tensile strength is expected to relate linearly with the interparticle adhesion force [12], it leads us again to the

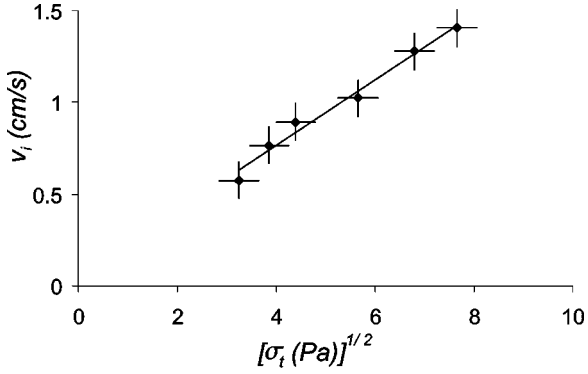

FIG. 9. Measured interstitial gas velocity for a homogeneous fluidization state ($\phi = 0.15$) as a function of the square root of the tensile strength of the packed bed. The continuous line is a linear fit to the data.

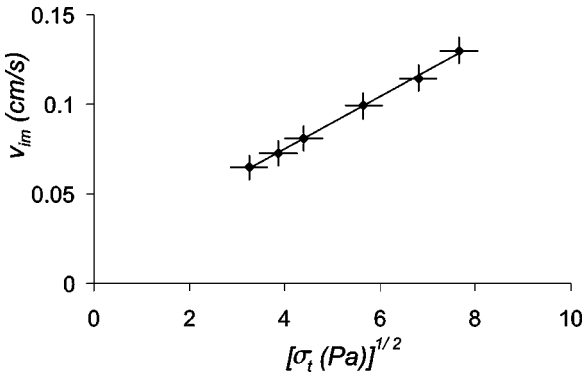

FIG. 10. Computed interstitial gas velocity at incipient fluidization from experimental measurements of the packed solid volume fraction and tensile strength as a function of the square root of the tensile strength.

conclusion that the interstitial gas velocity must scale as the square root of the powder tensile strength of the packed bed.

Another characteristic gas velocity is the minimum fluidization velocity v_{sm}, defined as the superficial gas velocity at which the pressure drop balances the weight of the powder bed per unit area (σ_c) plus its tensile strength. The pressure drop across the powder at the point of incipient fluidization is then given by $\Delta P_m = \sigma_c + \sigma_t$. At low Reynolds numbers the gas flow through the packed bed is laminar and the pressure drop is a linear function of the superficial gas velocity (Carman-Kozeny law [14]):

$$\frac{\Delta P}{h} = \frac{E\mu}{d_p^2} \frac{\phi_p^2}{(1-\phi_p)^3} v_s, \tag{6}$$

where μ is the dynamic gas viscosity ($\mu = 1.89 \times 10^{-5}$ Pa s at ambient temperature), v_s is the superficial gas velocity, ϕ_p is the solid volume fraction of the packed bed, $E \sim 200$ is an empirical constant, and h is the powder bed height that is related to $\phi_p [h = \sigma_c / (\rho_p g \phi_p)]$. The gas velocity needed for fluidization is derived by imposing the condition $\Delta P(v_{sm}) = \Delta P_m$,

$$v_{sm} = \frac{\rho_p g d_p^2}{E\mu} \frac{(1-\phi_p)^3}{\phi_p} \left[1 + \frac{\sigma_t}{\sigma_c} \right], \tag{7}$$

and the interstitial gas velocity at incipient fluidization is simply given by $v_{im} = v_{sm}/(1-\phi_p)$. Results for v_{im} obtained from the measured values of ϕ_p and σ_t are represented in Fig. 10. Again, the trend found for the interstitial gas velocity is quite close to a square root law of the powder tensile strength. Figures 9 and 10 also indicate that the interstitial gas velocity for a solid volume fraction of 0.15, close to the bubbling regime, is about one order of magnitude larger than the minimum gas velocity needed for fluidization, and this result has been confirmed by direct measurements of both characteristic velocities in samples of different powders.

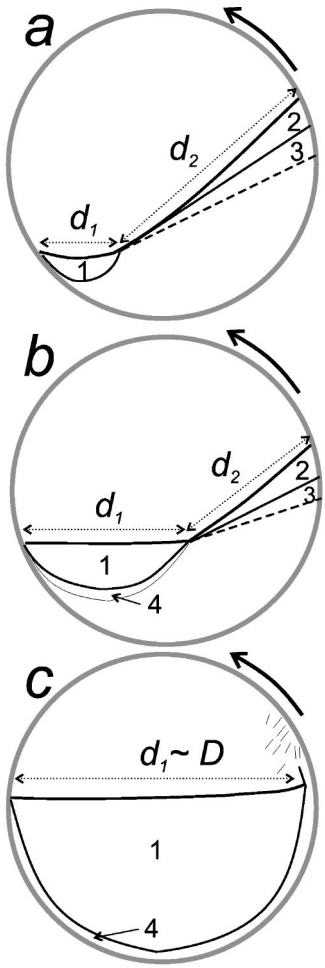

FIG. 11. Physical model on the fluidization-defluidization process.

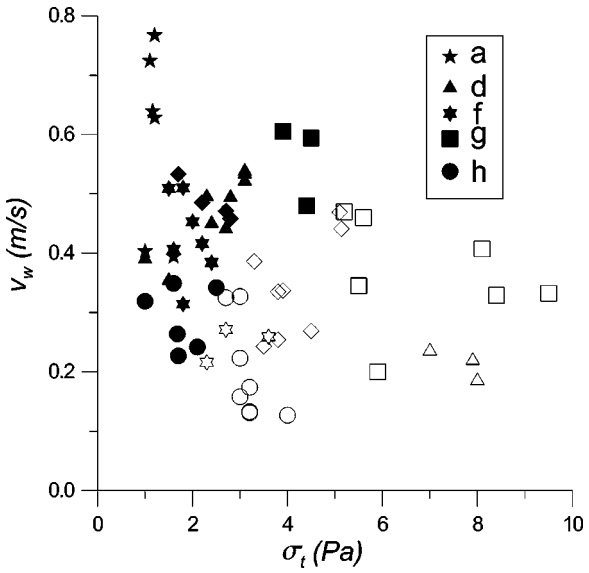

FIG. 12. Avalanching wedge velocity as a function of the average wedge tensile strength from tilted bed experiments and for different samples of powder. For solid symbols the wedge fluidizes upon impact on the wall, whereas for open symbols it remains in the plastic regime.

A. Physical model

We are now in a position to postulate a physical model for the fluidization and defluidization processes in the rotating drum that provides us with a rationale for understanding the physical basis of the above nondimensional numbers. Figure 11 represents three typical stages of the fluidization process as we increase the angular velocity. In Fig. 11(a), which corresponds to Fig. 1(a), the wedge of powder, consisting of parts 2 and 3, avalanches. As a result of the impact on the wall part 2 of the wedge is fluidized, but before the next avalanche takes place the entrapped air has time to escape and the material ends up in a plastic state with a horizontal surface. This interpretation is backed by independent measurements of the quasistatic avalanching process made in a tilted bed of rectangular shape [15]. In these experiments the material is first initialized by fluidization. After shutting off the gas supply the material collapses under its own weight with a horizontal free surface. Once the material has collapsed, the bed is tilted slowly until an avalanche is triggered and a slice of powder slides down the slope formed by the rest of the material. If the material in the slice is fluidized during the avalanche, it will behave like a liquid as it comes to rest with a horizontal free surface. Recording the experiment with the CCD camera makes it possible to measure the average velocity of the slice during the avalanche (v_w). As we know from other experiments the tensile strength of the materials used in this experiment, we know for each avalanche the tensile strength of the material in the slice and its velocity and we can make a plot like the one in Fig. 12. This figure shows that in order to become fluidized during an avalanche, the velocity of the slice must overcome a certain threshold that depends on the tensile strength of the material in the slice.

In Fig. 11(b) the model corresponds to the situation of Fig. 1(b). Avalanching is now a practically continuous process. The falling mass during a time interval Δt scales as $\Delta m_f \sim d_2 \omega R \Delta t$. Since the process is stationary, the same amount of mass is defluidized in the same time interval and settles in part 4. The settling velocity can be estimated as the gas velocity and thus the defluidized mass scales as $\Delta m_{df} \sim d_1 v_i \Delta t \sim \Delta m_f$. Since the interstitial gas velocity in the fluidized region (part 1) of the bed grows as the square root of the tensile strength, we obtain $d_1/d_2 \sim \omega R/\sqrt{\sigma_t} \propto \sqrt{\Theta}$. Thus, it turns out that the parameter Θ is a natural parameter to describe the evolution of the powder.

Finally, Fig. 11(c) corresponds to Fig. 1(c), and shows the onset of fluidization. The powder that sediments in one rotation period (part 4) is the powder that comes out at the right side pulverized. The sediment thickness is proportional to $R v_i \Delta t$, and it is ejected with velocity ωR during the time Δt, through a length $d_2 = \alpha R$ (from Fig. 1 we see that α must be of order 10^{-1} or smaller). Therefore, at the onset of fluidization v_i must be proportional to ωR. Due to the relation between v_i and σ_t and the negligible variation of the initial density of our powders, we may choose again Θ as a suitable parameter to characterize this transition.

VI. CONCLUSIONS

In conclusion, we have found that for a set of powders of varying cohesiveness and for different geometries, fluidization is universally ruled by the ratio of the kinetic energy density to the powder tensile strength. Moreover the estimated average interstitial gas velocity scales with the tangential rotation velocity. This scaling implies that the interstitial gas velocity should increase as the square root of the powder tensile strength, and this has been confirmed by independent measurements using a powder bed technique.

As a final remark we want to emphasize that for the powders used in this experiment the onset of fluidization, defined as the lowest angular velocity at which the free surface of the material becomes horizontal ($d/D \sim 1$), occurs at a value $\Theta \sim 1$ (Fig. 7). Given the different particle sizes, cohesiveness, and drum diameters, we may expect that a useful design rule for industry applications involving fluidization of fine cohesive powders in rotating drums should be $\Theta \sim 1$.

ACKNOWLEDGMENTS

This research was supported by the Xerox Foundation, Spanish Government Agency Ministerio de Ciencia y Tecnologia (DGES) under Contract No. BMF2000-1056, and NATO Grant No. LINKAGE PST.CLG.976575.

[1] K. Rietema, *The Dynamics of Fine Powders*, (Elsevier, Amsterdam, 1991), pp. 233–237.
[2] A. Castellanos, J.M. Valverde, A.T. Pérez, A. Ramos, and P.K. Watson, Phys. Rev. Lett. **82**, 1156 (1999).
[3] K.M. Hill, A. Caprihan, and J. Kakalios, Phys. Rev. Lett. **78**, 50 (1997).
[4] H.M. Jaeger, C.-h. Liu, and S. Nagel, Phys. Rev. Lett. **62**, 40 (1989).
[5] M. Nakawa, S.A. Altobelli, A. Caprihan, E. Fukushima, and E.K. Jeong, Exp. Fluids **16**, 54 (1993).
[6] M.A.S. Quintanilla, J.M. Valverde, A. Castellanos, and R.E. Viturro, Phys. Rev. Lett. **87**, 194301 (2001).
[7] J.M. Valverde, A. Castellanos, A. Ramos, A.T. Perez, M.A. Morgan, and P.K. Watson, Rev. Sci. Instrum. **71**, 2791 (2000).
[8] J.M. Valverde, A. Castellanos, and M.A.S. Quintanilla, Phys. Rev. Lett. **86**, 3020 (2001).
[9] M.A.S. Quintanilla, A. Castellanos, and J.M. Valverde, Phys. Rev. E **64**, 031301 (2001).
[10] S. Ross and I.D. Morrison, *Colloidal Systems and Interfaces* (Willey Interscience, New York, 1988).
[11] J.R. Wank, S.M. Georg, and A.W. Weimer, Powder Technol. **121**, 195 (2001).
[12] A. Castellanos, J.M. Valverde, and M.A.S. Quintanilla, Phys. Rev. E **64**, 041304 (2001).
[13] T.A. Witten and L.M. Sander, Phys. Rev. Lett. **47**, 1400 (1981).
[14] P.C. Carman, Trans. Inst. Chem. Eng. **15**, 150 (1937).
[15] J.M. Valverde, A. Castellanos, A. Ramos, and P.K. Watson, Phys. Rev. E **62**, 6851 (2000).